1,3-dioxolan-2-one and dialkylamine at 60 °C for 22 h,[12,15] followed by distillation under reduced pressure.

Measurements. ^1H and ^{13}C NMR spectra were measured on a JEOL JNM-GX 400 FT NMR spectrometer. Infrared spectra were measured with a Hitachi 260-30 infrared spectrophotometer. Gas chromatography was carried out on an Ohkura Gas Chromatograph Model-103 equipped with a glass capillary column of 30 m × 0.28 mm; adsorber, silicone SF-96.

Registry No. $TPPH_2$, 917-23-7; **1** (X = Et), 63256-30-4; **1** (X = O_2CCH_3), 85709-47-3; **4** (R = R′ = Me; R″ = Et), 99547-43-0; **6** (R_1 = Me; R_2 = H), 37499-12-0; **6** (R_1 = Et; R_2 = H), 99532-93-1; **6** (R_1 = Ph; R_2 = H), 99532-94-2; **6** (R_1 = CH_2OMe; R_2 = H), 99532-95-3; **6** (R_1 = R_2 = Me), 99532-96-4; **6** (R = *i*-Pr), 99532-98-6; **6** (R = $(-CH_2-)_5$), 99532-99-7; **7** (R_1 = Me; R_2 = H), 4402-32-8; **7** (R_1 = Et; R_2 = H), 2683-58-1; **7** (R_1 = Ph; R_2 = H), 4249-64-3; **7** (R_1 = CH_2OMe; R_2 = H), 3141-80-8; **7** (R_1 = R_2 = Me), 99532-97-5; **7** (R = *i*-Pr), 2109-63-9; $AlEt_3$, 97-93-8; $\overline{CH(Me)CH_2O}$, 75-56-9; $\overline{CH(Et)CH_2O}$, 106-88-7; $\overline{CH(Ph)CH_2O}$, 96-09-3; $CH(CH_2OMe)CH_2O$, 930-37-0; (*cis*)-$\overline{CH(Me)CH(Me)O}$, 1758-33-4; $HNEt_2$, 109-89-7; $HN(Pr\text{-}i)_2$, 108-18-9; CO_2, 124-38-9; NHMe(CH_2Ph), 103-67-3; piperidine, 110-89-4.

(15) Katzhendler, J.; Ringel, I.; Sarel, S. *J. Chem. Soc., Perkin Trans. 2* **1972**, 2019.

Dynamics of Spin-State Interconversion and Cooperativity for Ferric Spin-Crossover Complexes in the Solid State. 5.[1] Variable-Temperature Spectroscopic, Magnetic, and Single-Crystal X-ray Structural Characterizations of the Spin-State and Order–Disorder Transformations of a Schiff Base Complex

Mark D. Timken,[2] Charles E. Strouse,*[3] S. Michael Soltis,[3] Stephen A. Daverio,[3] David N. Hendrickson,*[2] A. M. Abdel-Mawgoud,[2,4] and Scott R. Wilson[2]

Contribution from the School of Chemical Sciences, University of Illinois, Urbana, Illinois 61801, and Department of Chemistry and Biochemistry, University of California, Los Angeles, California 90024. *Received June 12, 1985*

Abstract: Two types of solid-state structural dynamics are exhibited by $[Fe(3\text{-}OEt\text{-}SalAPA)_2]ClO_4 \cdot C_6H_6$, where 3-OEt-SalAPA is the monoanion of the Schiff base condensate of 3-ethoxysalicylaldehyde and *N*-(3-aminopropyl)aziridine. Variable-temperature magnetic susceptibility and EPR data show that the compound undergoes a gradual, but complete, spin-crossover transformation for which there are equal populations of high- and low-spin complexes at 205 K. Only a single quadrupole-split doublet is seen in the Mössbauer spectrum at all temperatures from 111 to 306 K. Thus, this complex is interconverting between low- and high-spin states at a rate faster than the inverse of the Mössbauer time scale. No hysteresis is seen in any of the spectroscopic or magnetic measurements. A multiple-temperature structural investigation has provided an independent characterization of the spin transformation. This characterization is in complete accord with the magnetic data but reveals a second structural transformation whose presence is not reflected in the spectroscopic or magnetic data. This second transformation, at about 180 K, is an order–disorder transformation which results in a change of space group from $C2/c$ at high temperature to $P2_1/c$ at low temperature. The abrupt nature of this transformation, the observed hysteresis (ΔT = 15 K), and the observation of two phases in the hysteresis region are characteristic of a first-order transition. The order–disorder transformation involves a dynamic interconversion of two crystallographically distinct sites. Preservation of the local environments at the two iron sites accounts for the insensitivity of the spin-equilibrium thermodynamics to the transformation. Although the X-ray investigation provides no direct evidence of the rate of interconversion between the two environments, the possible influence of this dynamic process on the rate of spin-state interconversion is discussed.

Solid-state spin-crossover transformations have been of recent interest because they provide a means for investigating just how an intramolecular process (the spin-state interconversion) is coupled to the intermolecular interactions intrinsic to a condensed phase. To date, research in this area[5-8] has centered to a greater extent on the solid-state factors that influence the thermodynamics at the spin-crossover transformation and to a lesser extent on the factors that influence spin-state interconversion rates. In fact, very little is known about the role of intermolecular interactions in inhibiting or enhancing these rates in the solid state. Within the past few years, several ferric spin-crossover solids have been discovered which may provide new insights into this problem.

In two of the preceding papers[9,10] in this series the magnetic and spectroscopic properties of the new ferric N_4O_2 spin-crossover

(1) Part 4 in the series: Timken, M. D.; Wilson, S. R.; Hendrickson, D. N. *Inorg. Chem.* **1985**, *24*, 3450.
(2) University of Illinois.
(3) University of California, Los Angeles.
(4) On leave from Faculty of Sciences at Sohag, Egypt.
(5) Kõnig, E.; Ritter, G.; Irler, W.; Goodwin, H. A. *J. Am. Chem. Soc.* **1980**, *102*, 4681.
(6) König, E.; Ritter, G.; Kulshreshtha, S. K.; Nelson, S. M. *J. Am. Chem. Soc.* **1983**, *105*, 1924.
(7) Purcell, K. F.; Edwards, M. P. *Inorg. Chem.* **1984**, *23*, 2620.
(8) Gütlich, P. *Struct. Bonding (Berlin)* **1981**, *44*, 83.
(9) Federer, W. D.; Hendrickson, D. N. *Inorg. Chem.* **1984**, *23*, 3861.
(10) Federer, W. D.; Hendrickson, D. N. *Inorg. Chem.* **1984**, *23*, 3870.

0002-7863/86/1508-0395$01.50/0

Table I. Crystallographic Data for $[Fe(3\text{-}OEt\text{-}SalAPA)_2]ClO_4 \cdot Benzene$

	20 K[a]	128 K[a]	175 K[a]	298 K[a]	300 K[b]
a, Å	16.55 (3)	16.54 (1)	16.732 (5)	16.960 (4)	16.935 (4)
b, Å	17.22 (3)	17.35 (1)	17.501 (5)	17.600 (4)	17.602 (4)
c, Å	13.41 (2)	13.46 (1)	13.578 (3)	13.832 (3)	13.802 (3)
β, deg	119.60 (2)	119.267 (8)	119.08 (1)	119.030 (5)	119.08 (1)
V, Å^3	3323	3370	3474	3610	3596
D, g/cm^3	1.46	1.43	1.39	1.34	1.35
crystal size, mm	0.05 × 0.10 × 0.20	0.18 × 0.18 × 0.31	0.24 × 0.25 × 0.41	0.18 × 0.18 × 0.31	0.38 × 0.39 × 0.85
2θ max, deg	50	50	50	50	55
Z	4	4	4	4	4
space group	$P2_1/c$	$P2_1/c$	$P2_1/c$	$C2/c$	$C2/c$
total reflections	6334	6306	6566	6723[c]	4131
obsd reflections	2571 (3σ)	3654 (3σ)	3336 (3σ)	1318 (3σ)	2589 (2.58σ)
diffractometer[d]	Huber	Picker	Huber	Picker	Syntex
R[e]	0.079	0.062	0.077	0.071	0.052
R_w[e]	0.090	0.072	0.092	0.082	0.070
EOF	1.959	1.951	2.478	2.134	2.36

[a] Performed at UCLA. [b] Performed at Illinois. [c] Collected in a primitive cell. [d] Graphite monochromatized Mo Kα radiation. [e] $R = (\sum||F_o| - |F_c||/\sum|F_o|)$; $R_w = (\sum w||F_o| - |F_c||^2/\sum w|F_o|^2)^{1/2}$, where F_o and F_c are observed and calculated structure factors, respectively, and $w = 1/\sigma^2(F_o)$.

complex $[Fe(SalAPA)_2]ClO_4$, where SalAPA is the monoanion of the Schiff-base condensate of salicylaldehyde and aminopropylaziridine, were described. The complex, in its unsolvated and CH_2Cl_2-solvated forms, was shown to be a member of the relatively new class of ferric N_4O_2 spin-crossover solids which undergo rapid spin-state interconversion on the Mössbauer time scale. Other members of this class are the complexes recently reported by Maeda et al.[11-14] Previously, only the ferric dithiocarbamates,[15] monothiocarbamates,[16] and diselenocarbamates[17] were shown to interconvert rapidly relative to the Mössbauer time scale. The spin-state interconversion rates in these FeN_4O_2 systems appear to be sensitive to relatively subtle solid-state effects. Maeda et al. have established that counterion[14] and ligand substitutent[13] changes can dramatically alter the nature of the observed Mössbauer spectra. Unfortunately, the exact origins of these effects are unknown.

In this paper the variable-temperature magnetic, spectroscopic, and structural characterizations of the spin-crossover transformation are reported for $[Fe(3\text{-}OEt\text{-}SalAPA)_2]ClO_4 \cdot C_6H_6$, where 3-OEt-SalAPA is identical with the SalAPA ligand except for addition of the 3-ethoxy substituent on the salicylaldehyde ring. In addition to a spin equilibrium, this material exhibits an order–disorder transformation in the neighborhood of 180 K. The disorder in the high-temperature phase involves interconversion between two nonequivalent iron ion environments. Although no information is yet available concerning the rate of this "exchange", the possibility arises that this dynamic feature of the structure enhances the rate of spin-state interconversion.

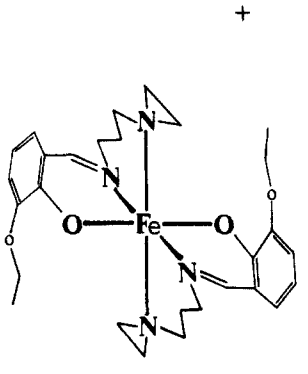

Experimental Section

Compound Preparation. Reagents were obtained as described previously by Federer.[9] The ^{57}Fe powder (95% enriched) was obtained from New England Nuclear. Elemental analyses were performed in the Microanalytical Laboratory of the School of Chemical Sciences, University of Illinois.

The precursor $[Fe(3\text{-}OEt\text{-}SalAPA)_2]ClO_4$ was prepared exactly as described previously[9] for $[Fe(SalAPA)_2]ClO_4$, except that 3-ethoxysalicylaldehyde was used in place of salicylaldehyde.

The benzene solvate was obtained by recrystallization of the precursor in methylene chloride/benzene. In a typical preparation, 20 mg of $[Fe(3\text{-}OEt\text{-}SalAPA)_2]ClO_4$ was dissolved in 4 ml of CH_2Cl_2. After the dropwise addition with stirring of 3 mL of benzene, the deep purple solution was allowed to stand. Within a few minutes to a few hours, deep purple crystals formed which were isolated by filtration, washed with ether, and air dried. Large crystals isolated in this manner were used for single-crystal structural studies. Anal. Calcd for $^{57}FeC_{36}H_{42}N_5O_7$: C, 56.00; H, 6.08; N, 7.68. Found: C, 55.27; H, 6.36; N, 7.60.

Methods. Variable-temperature magnetic susceptibility data were obtained on a series 800 VTS-50 SQUID susceptometer (S.H.E. Corp.) maintained by the Physics Department, University of Illinois. A magnetic field of 10 kG was used. Diamagnetic corrections, estimated from Pascal's constants, were used in the calculation of molar paramagnetic susceptibilities.

Electron paramagnetic resonance data at X-band frequency (9.1 GHz) were collected on a Varian E-9 spectrometer. Variable temperatures (300–130 K) were obtained with the use of a gas-flow cavity insert and a Varian V-4540 temperature controller. Temperatures are accurate to 5 K. A direct immersion dewar was used to obtain spectra at 77 K. Spectra below 77 K were obtained on a Bruker ER-200D spectrometer equipped with an Oxford cavity insert. Q-band (35 GHz) spectra were collected on a Varian E-15 spectrometer; low temperatures were achieved by inserting the entire cavity into a gas-flow cryostat.

Mössbauer data were collected on a previously described[18] apparatus. The sample temperatures, controlled by a Lake Shore Cryotronics Model DRC 80C temperature controller in conjunction with a silicon diode mounted on the copper sample cell holder, are estimated to have an absolute accuracy of 3 K. Because of the poor recoilless fraction intrinsic to these compounds, samples enriched to 95% in ^{57}Fe were used. Sample sizes ranged from 3 to 8 mg. The Mössbauer data were computer fit to Lorentzian line shapes with the use of a previously described[19] program. The isomer shift values are reported relative to iron foil at 298 K but are not corrected for the temperature-dependent second-order Doppler shift.

X-ray powder diffraction patterns were obtained with the use of a Norelco (Phillips Electronics Co.) powder diffractometer equipped with a copper X-ray tube and a graphite monochromator.

Room-Temperature Crystal Measurements and Data Collection. An opaque blue prismatic crystal of $[Fe(3\text{-}OEt\text{-}SalAPA)_2]ClO_4 \cdot C_6H_6$ (0.38 × 0.39 × 0.85 mm) was used for data collection at the University of Illinois. The unit cell parameters, listed in Table I, were obtained by a least-squares fit to the automatically centered settings for 15 reflections. Details of data collection may also be found in Table I. The crystal

(11) Maeda, Y.; Tsutsumi, N.; Takashima, Y. *Chem. Phys. Lett.* **1982**, *88*, 248.
(12) Maeda, Y.; Ohshio, H.; Takashima, Y. *Chem. Lett.* **1982**, 943.
(13) Ohshio, H.; Maeda, Y.; Takashima, Y. *Inorg. Chem.* **1983**, *22*, 2684.
(14) Maeda, Y.; Tsutsumi, N.; Takashima, Y. *Inorg. Chem.* **1984**, *23*, 2440.
(15) Merrithew, P. B.; Rasmussen, P. G. *Inorg. Chem.* **1972**, *11*, 325.
(16) Kunze, K. R.; Perry, D. L.; Wilson, L. J. *Inorg. Chem.* **1977**, *16*, 594.
(17) DeFilipo, D.; Depalano, P.; Diaz, A.; Steffe, S.; Trogu, E. F. *J. Chem. Soc. Dalton* **1977**, 1566.
(18) Cohn, M. J.; Timken, M. D.; Hendrickson, D. N. *J. Am. Chem. Soc.* **1984**, *106*, 6683.
(19) Chrisman, B. L.; Tumolillo, T. A. *Comput. Phys. Commun.* **1971**, *2*, 322.

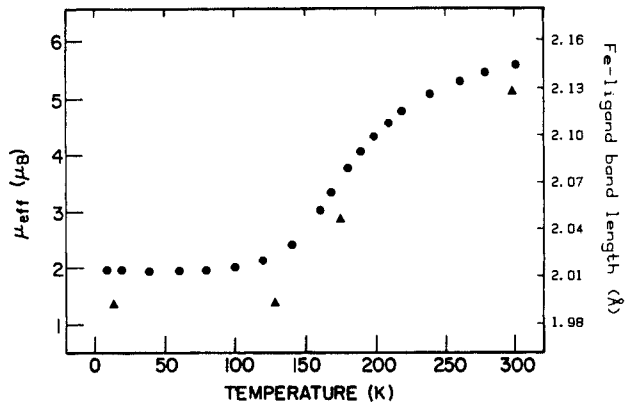

Figure 1. Effective magnetic moment (●) and the average iron–ligand bond length (▲) vs. temperature for $[Fe(3\text{-}OEt\text{-}SalAPA)_2]ClO_4$·benzene.

diffracted well to $2\theta = 50°$. There were no remarkable changes in the appearance of the sample during data collection. The data were corrected for Lorentz and polarization effects. A numerical absorption correction ($\mu = 5.63$ cm^{-1}) was applied with maximum and minimum transmission coefficients of 0.851 and 0.786.

Low-Temperature Data Collection. Low-temperature data sets were collected at UCLA from three different crystals, details of which are listed in Table I. The 128 K data set was collected on a locally modified Picker diffractometer with a gas stream low-temperature device. The crystal was mounted on a glass fiber. The 20 and 175 K data sets were collected on a locally automated Huber diffractometer with a prototype version of a closed-cycle low-temperature device based on an Air Products Model 202 refrigerator. In each case the crystals were mounted directly on a copper pin attached to the end of the refrigerator. The uncertainty in the temperature of the "20 K" data set is on the order of 5 K. This uncertainty arises from the lack of a radiation shield around the crystal in this prototype. The small size of the crystal used in this collection contributed to relatively large uncertainties in the lattice parameters obtained. The use of a larger crystal for the 175 K data set improved the quality of both the lattice parameters and the measured intensities. Structure factors were derived from an analysis of the peak scan profiles.[20]

Structure Solution and Refinement. Direct methods (MULTAN) were used to solve the room-temperature structure in the space group $C2/c$. Correct positions for 19 of the 25 non-hydrogen atoms were deduced from an E map. Subsequent difference Fourier calculations gave positions for the remaining non-hydrogen atoms. In the final cycles of full-matrix least squares, all non-hydrogen atoms were refined with anisotropic thermal coefficients, and a group isotropic thermal parameter was refined for the hydrogen atoms which were fixed in idealized positions. Tables of the observed and calculated structure factors are available.[21] The thermal coefficients for atoms O4, C15, C16, and C17 converged to abnormally high values and the bonded contacts for these atoms appear artificially short.

While the lattice parameters obtained at 128 K are similar to those observed at room temperature, the lack of three-dimensional systematic absences at 128 K is indicative of a primitive ($P2_1/c$) rather than a C-centered cell. The $P2_1/c$ structure was solved by conventional heavy-atom methods and refined by full-matrix least squares. Experimental parameters associated with the structural determinations are tabulated in Table I, including those for a parallel room-temperature determination conducted at UCLA.

Results and Discussion

The Spin-Crossover Transformation; Magnetism and Spectroscopy. As is evident in Figure 1, $[Fe(3\text{-}OEt\text{-}SalAPA)_2]ClO_4\cdot C_6H_6$ shows a gradual and nearly complete thermal spin-crossover transformation. Assuming μ_{eff}(H.S.) = 5.99 μ_B and μ_{eff}(L.S.) = 1.90 μ_B, the high-spin fraction at 300 K is 0.846, at 200 K it is 0.535, and at 79 K it is 0.006. The susceptibility data, with the use of the above assumptions, were converted into equilibrium constant data, where K_{eq} = (fraction high spin)/(1 - fraction high spin). A plot of the natural logarithm of K_{eq} vs. reciprocal temperature gives a very linear relationship in the temperature range of 140–300 K. Over this linear region, which encompasses more than 77% of the spin-crossover transformation, the thermodynamic parameters ΔH = 2.24 kcal/mol and ΔS = 10.9 eu were obtained.

The gradual and nearly complete nature of the spin-crossover transformation is also evident from the variable-temperature EPR results (Figure 2). It is clear that as the temperature of the sample

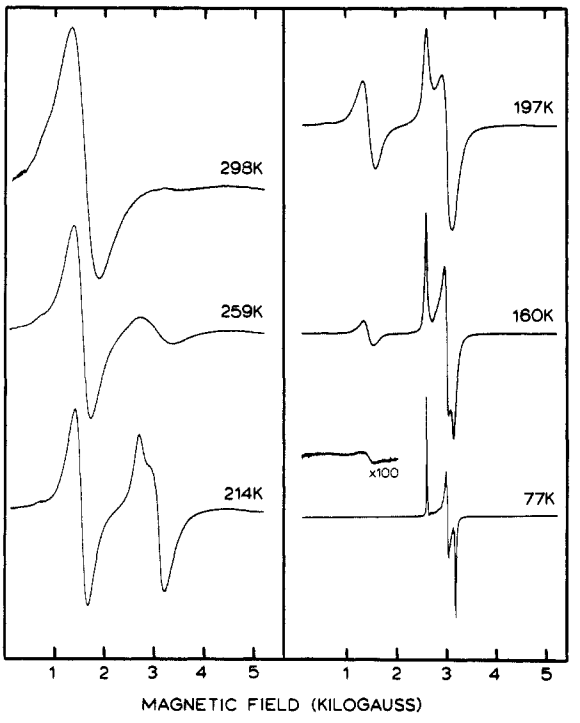

Figure 2. X-band (9.1 GHz) spectra of $[Fe(3\text{-}OEt\text{-}SalAPA)_2]ClO_4$· benzene.

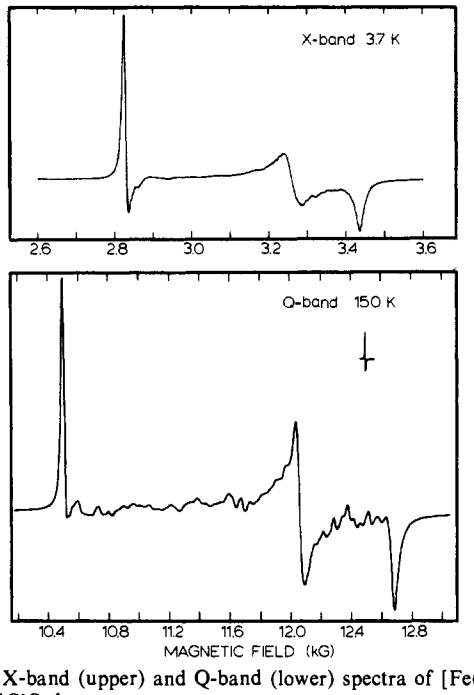

Figure 3. X-band (upper) and Q-band (lower) spectra of $[Fe(3\text{-}OEt\text{-}SalAPA)_2]ClO_4$·benzene.

(20) The programs used in this work included modified versions of the following programs: CARESS (Broach, Coppens, Becker and Blessing), peak profile analysis, Lorentz and polarization corrections; MULTAN (Main), package of programs, including direct methods, structure factor normalization, Fourier transform, and peak search; ORFLS (Busing, Martin and Levy), structure factor calculation and full-matrix least-squares refinement; ORFFE (Busing, Martin, and Levy), distance, angle, and error calculations; ABSORB (Coppens, Edwards and Hamilton), absorption correction calculation; ORTEP (Johnson) figure plotting; HYDROGEN (Trueblood), calculation of hydrogen atomic positions. All calculations were performed on a DEC VAX 11/750 crystallographic computer. Scattering factors and corrections for anomalous dispersion were taken from the following: "International Tables for X-ray Crystallography"; Kynoch Press: Birmingham, England, 1974; Vol. 10.

(21) Supplementary material.

Table II. Mössbauer Parameters for $Fe(3\text{-}OEt\text{-}SalAPA)_2ClO_4$·Benzene (2-Line Lorentzian Fits)[a]

T, K	i.S., mm/s	Q.S., mm/s	Γ_-,[b] mm/s	Γ_+,[c] mm/s	ln area[d]	χ^{2e}
306[f]	0.317 (1)	1.481 (3)	0.332 (2)	0.508 (3)	1.090	1.02
274[f]	0.337 (2)	1.381 (3)	0.402 (2)	0.616 (4)	1.510	1.65
245[f]	0.365 (2)	1.267 (5)	0.466 (3)	0.728 (6)	1.841	4.28
224[f]	0.348 (2)	1.199 (4)	0.483 (3)	0.737 (6)	1.995	4.57
205[f]	0.334 (2)	1.284 (4)	0.520 (3)	0.699 (5)	1.797	1.33
195[g]	0.322 (1)	1.414 (3)	0.534 (2)	0.663 (3)	1.881	1.30
185[g]	0.314 (1)	1.600 (3)	0.545 (3)	0.616 (3)	1.970	1.21
173[g]	0.309 (1)	1.792 (2)	0.556 (2)	0.600 (3)	2.067	1.37
159[g]	0.291 (1)	2.084 (2)	0.462 (2)	0.453 (2)	2.152	3.52
145[g]	0.284 (1)	2.274 (2)	0.371 (2)	0.342 (2)	2.199	4.18
129[g]	0.282 (1)	2.360 (3)	0.307 (3)	0.279 (2)	2.209	6.71
111[g]	0.287 (1)	2.389 (3)	0.277 (3)	0.254 (3)	2.219	10.5

[a] Parameters obtained assuming equal areas for the two-component peaks of the quadrupole doublet. [b] Half-width at half-height of the negative velocity component. [c] Half-width at half-height for the positive velocity component. [d] Natural logarithm of background-normalized area of the total fitted spectrum. [e] χ^2 value indicating quality of data and of fit to six adjustable parameters. [f] 8-mg sample size. [g] 5-mg sample size.

is decreased the low-spin signal (g = 2, 3000 G) increases in intensity at the expense of the high-spin signal (g = 4, 1500 G). These high- and low-spin EPR signals are typical for ferric centers of this type and are very similar to what was found in the previous papers[9,10] in this series. The g = 4 resonance is characteristic of a high-spin ferric center in a rhombically distorted ligand environment. In Figure 3 an expanded view of the low-spin ferric region is presented. Because of the extremely crystalline nature of this material, and because of our wish to avoid the spurious effects of sample grinding, the spectra show some evidence for crystalline orientation. However, the presence of only three major **g**-tensor components is quite clear. These **g**-tensor components (g_1 = 2.379, g_2 = 2.077, g_3 = 1.974) have been analyzed by following the method of Bohan.[22] This analysis indicates that the first excited spin-doublet electronic state is at least 5000 cm^{-1} higher in energy than the ground state. This result is important in that it predicts a temperature-independent low-spin ferric magnetic moment and a temperature-independent low-spin Mössbauer quadrupole splitting. Consequently, we can attribute the temperature-dependent changes in these observables primarily to the spin-crossover transformation. The details of the **g**-tensor analysis will be presented in a subsequent report.[23] It is also important to note that because distinct high- and low-spin EPR signals are evident, we can conclude that the intramolecular spin-state interconversion lifetime is longer than ca. 10^{-9} s, as estimated from the line width in the 214 K spectrum.

Variable-temperature Mössbauer data, shown in Figure 4 and listed in Table II, are consistent with the gradual nature of the spin-crossover transformation. The solid lines in the figure represent computer fittings to Lorentzian line shapes. In contrast to the EPR results, only a single population-weighted average signal is evident; the interconversion is rapid on the Mössbauer time scale.

At low temperature (111 K), the quadrupole splitting and isomer shift values are typical for those of a low-spin ferric center. The high-spin fraction increases and the quadrupole splitting decreases as the temperature is increased to 220 K. Above this temperature, however, the quadrupole splitting increases despite the increase in the high-spin fraction. This minimum in quadrupole splitting vs. temperature, illustrated in Figure 5, was initially surprising but has been noted before.[9-14] As discussed in theoretical terms by Maeda,[24] such behavior is expected if the signs of the electric field gradient (EFG) tensor principal axis components (V_{zz}) for the low- and the high-spin electronic states are opposite. This prediction can also be understood with the use of simple quantitative arguments. In these arguments we will assume initially that the high- and low-spin EFG tensors are each axially symmetric and that the principal axis components, V_{zz}^H for the high-spin case and V_{zz}^L for the low-spin case, are colinear. Under

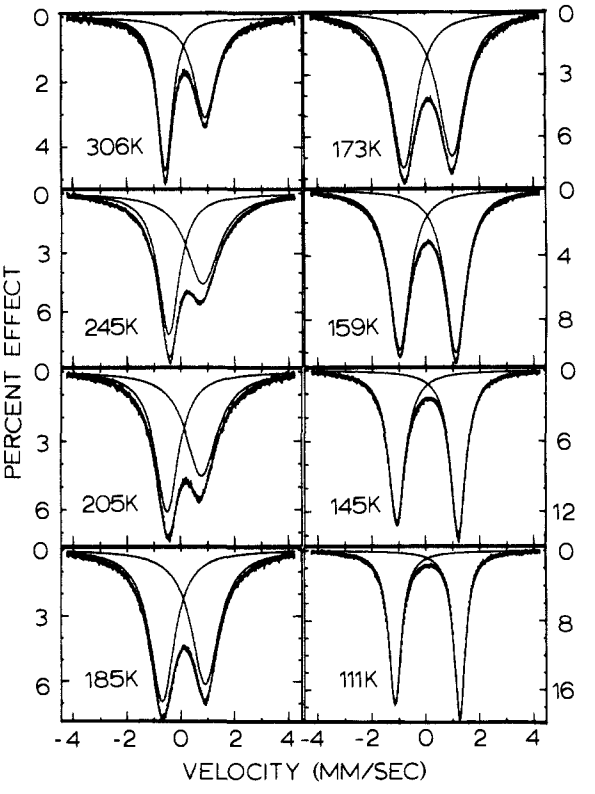

Figure 4. ^{57}Fe Mössbauer spectra of $[Fe(3\text{-}OEt\text{-}SalAPA)_2]ClO_4$·benzene at a number of temperatures.

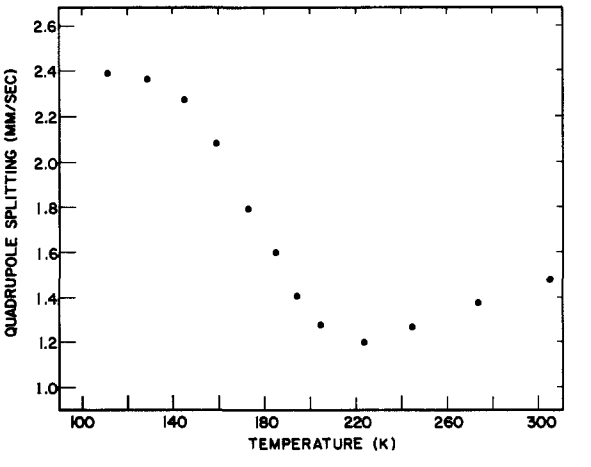

Figure 5. Mössbauer quadrupole splitting vs. temperature.

these assumptions, the quadrupole splitting value will be proportional to $[xV_{zz}^H + (1-x)V_{zz}^L]$, where x is the temperature-dependent fraction of high-spin molecules present and can vary

(22) Bohan, T. L. *J. Magn. Reson.* **1977**, *26*, 109.
(23) Timken, M. D.; Abdel-Mawgoud, A. M.; Hendrickson, D. N. *Inorg. Chem.*, in press.
(24) Maeda, Y.; Takashima, Y. *Mem. Fac. Sci., Kyushu Univ. Ser. C* **1983**, *14*, 107.

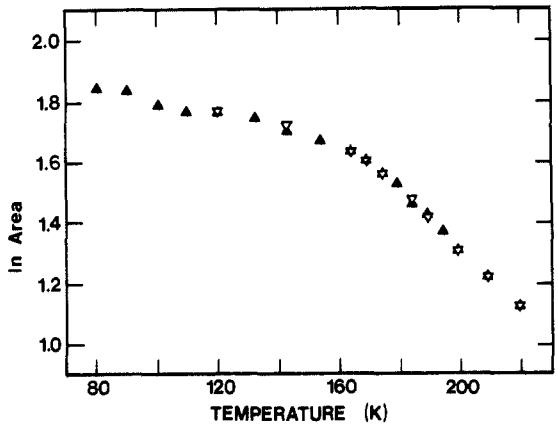

Figure 6. Natural logarithm of Mössbauer absorption area vs. temperature. Both heating (▲) and cooling (▽) curves are shown.

between 0 and 1. Equivalently, x is the fraction of time an individual molecule remains in the high-spin electronic state. In the case that V_{zz}^{H} and V_{zz}^{L} are oppositely signed, it is obvious that at some value of x (x(min)) a minimum quadrupole splitting will result. The predicted minimum is 0 mm/s, and x(min) is clearly related to the relative magnitudes of V_{zz}^{H} and V_{zz}^{L}. If we discard the assumptions of EFG tensor axial symmetry and colinearity of V_{zz}^{H} and V_{zz}^{L}, the important prediction, i.e., a minimum in the quadrupole splitting at some value of x, is still valid. However, in this case the quadrupole splitting minimum value will not necessarily be 0 mm/s. In fact, it is very likely that a nonzero minimum will now result. In addition, x(min) will now not only be a function of (V_{zz}^{H}/V_{zz}^{L}) but it will also depend upon precisely how the principal axes of the EFG tensors are aligned, as well as the extent of deviation of each tensor from axial symmetry. We believe that this predicted behavior corresponds to the curve illustrated in Figure 5.

In support of this conclusion, it is to be noted that the line width asymmetries of the essentially low-spin quadrupole doublet (111 K) and the essentially high-spin doublet (306 K) are opposite. That is, at 111 K the negative velocity component is the broader absorption, whereas at 306 K the positive component is broader. As discussed by Blume,[25] such asymmetry results when the paramagnetic relaxation is not sufficiently rapid relative to the ^{57}Fe nuclear Larmor precession frequency to average the internal magnetic field to zero over the lifetime of the nuclear excited state. The low-temperature asymmetry indicates that V_{zz}^{L} is negative, as expected for a low-spin d^5 (d_{xy} hole) ground state. The high-spin asymmetry indicates a positive V_{zz}^{H}. Again, these observations are consistent with the data illustrated in Figure 5. Although a quantitative reproduction of this curve is desirable, we do not presently have sufficient knowledge of the details of the EFG tensor nonaxiality and alignment to attempt such an analysis.

The line widths of the Mössbauer absorptions show somewhat unusual temperature dependencies. Evident from Figure 4 and Table II are the maxima in line widths which occur at 170 K for the negative velocity quadrupole component and at 220 K for the positive velocity component. Such line width maxima have been noted previously for rapidly interconverting ferric spin-crossover systems, and it has been suggested[9,10] that the maxima may be due to spin-state interconversion rates which exceed only slightly the Mössbauer spectroscopic time scale. However, in light of the incipient slow paramagnetic relaxation effects discussed in the preceding paragraph, in addition to the unknown temperature dependencies of these relaxation times, we cannot definitely assign the line width maxima to any single origin.

As a result of variable-temperature single-crystal X-ray structural observations discussed in more detail later in this paper, some of the spectroscopic and magnetic measurements were repeated in order to search for indications of thermal hysteresis. Variable-temperature magnetic susceptibility data, collected by cooling the sample from 300 to 10 K and warming back to 300 K, revealed no evidence for hysteresis. Mössbauer experiments were repeated in the order of 80 to 253 K then back to 121 K. No evidence for hysteresis was observed in either the quadrupole splitting or the Mössbauer absorption fraction (see Figure 6). Although small systematic differences were noted in the line widths, these differences were on the order of experimental uncertainties. Tabulations of all of the data referred to in this paragraph are included as supplementary material.

In Figure 6 is illustrated a plot of the natural logarithm of the Mössbauer absorption area vs. temperature. To a first approximation, there are two regions of linearity. In the high-temperature region (200–170 K), an effective Mössbauer temperature θ_M = 120 K was found (assuming the effective mass to be 57 amu), while in the low-temperature region (140–80 K) θ_M = 250 K. Apparently, the lattice undergoes a gradual change in its vibrational properties over the range of 140 to 170 K. Because the spin-crossover transformation begins in this region, it seems likely that this change is related to the spin-state transition.

While the observation of a single signal in the Mössbauer spectrum, indicative of "rapid" spin-state interconversion, served as the initial motivation of the detailed investigation of this material, the lack of information regarding the relative orientations of the EFG tensors in the two spin states (see above) precludes the quantitative determination of the interconversion rate from the Mössbauer data.

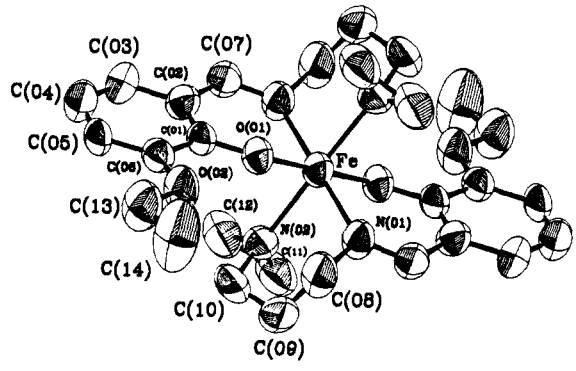

Figure 7. The molecular cation at 300 K.

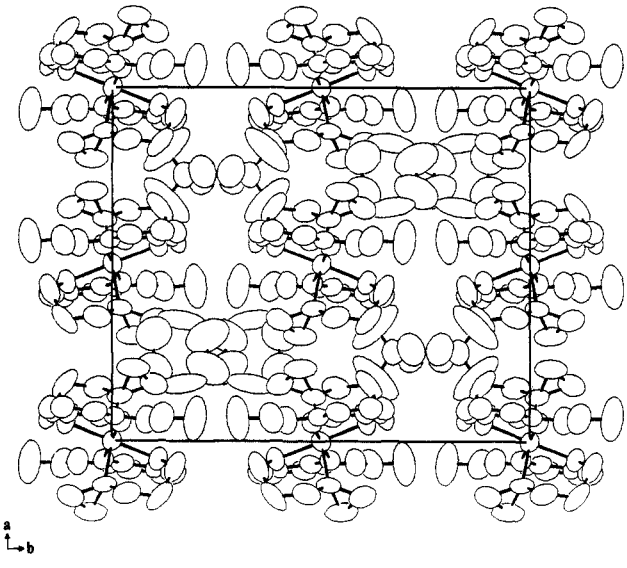

Figure 8. The packing diagram for the room-temperature structure viewed down the c axis.

The Room-Temperature Structure. Final positional and thermal parameters are listed in Table III, while Table IV contains selected bond lengths and angles. The structure and numbering system for the $[Fe(3\text{-}OEt\text{-}SalAPA)_2]^+$ cation are shown in Figure 7. Figure 8 shows the packing diagram viewed down the c axis.

In the $C2/c$ refinement, the complex ion is located on a crystallographic inversion center, while the perchlorate ion and the

(25) Blume, M. *Phys. Rev. Lett.* **1965**, *14*, 96.

Table III. Final Positional and Thermal Parameters (300 K)

	x/A	y/B	z/C
Fe	0.25	0.25	0.0
Cl	0.0	0.078256 (9)	0.25
O1	0.1955 (2)	0.2720 (1)	−0.1557 (2)
O2	0.1892 (2)	0.3325 (2)	−0.3315 (2)
O3	−0.0084 (3)	0.0325 (2)	0.1621 (3)
O4	0.0751 (6)	0.1186 (5)	0.2876 (6)
N1	0.1976 (2)	0.1406 (2)	−0.0445 (2)
N2	0.1246 (2)	0.2703 (2)	0.0032 (3)
C1	0.1855 (2)	0.2250 (2)	−0.2359 (3)
C2	0.1738 (2)	0.1464 (2)	−0.2328 (3)
C3	0.1586 (3)	0.0999 (3)	−0.3231 (3)
C4	0.1576 (3)	0.1308 (3)	−0.4140 (3)
C5	0.1690 (3)	0.2091 (3)	−0.4196 (3)
C6	0.1815 (2)	0.2559 (2)	−0.3330 (3)
C7	0.1694 (3)	0.1117 (2)	−0.1412 (3)
C8	0.1744 (4)	0.0994 (3)	0.0319 (4)
C9	0.0901 (4)	0.1347 (3)	0.0245 (4)
C10	0.1006 (3)	0.2157 (3)	0.0682 (4)
C11	0.0469 (3)	0.3004 (4)	−0.0961 (4)
C12	0.0930 (3)	0.3490 (3)	0.0015 (4)
C13	0.1839 (5)	0.3678 (3)	−0.4281 (4)
C14	0.1856 (7)	0.4489 (4)	−0.4113 (6)
C15	0.0394 (9)	0.3477 (6)	0.2566 (9)
C16	0.0834 (7)	0.4082 (7)	0.2650 (8)
C17	0.0431 (6)	0.4747 (6)	0.2583 (6)

	U_{11}	U_{22}	U_{33}	U_{23}	U_{13}	U_{12}
Fe	0.0476 (4)	0.0460 (4)	0.0314 (3)	−0.0055 (3)	0.0226 (3)	−0.0108 (3)
Cl	0.094 (1)	0.0647 (9)	0.0615 (8)	0.0	0.0493 (8)	0.0
O1	0.062 (1)	0.052 (1)	0.036 (1)	−0.0042 (9)	0.029 (1)	−0.006 (1)
O2	0.108 (2)	0.072 (2)	0.044 (1)	0.004 (1)	0.045 (2)	−0.005 (2)
O3	0.164 (4)	0.122 (3)	0.080 (2)	−0.024 (2)	0.074 (2)	−0.016 (3)
O4	0.357 (7)	0.381 (8)	0.175 (5)	−0.101 (5)	0.140 (5)	−0.285 (6)
N1	0.078 (2)	0.051 (2)	0.047 (2)	−0.007 (1)	0.037 (2)	−0.021 (2)
N2	0.050 (2)	0.088 (2)	0.044 (2)	−0.011 (2)	0.025 (1)	−0.008 (2)
C1	0.038 (2)	0.066 (2)	0.032 (2)	−0.005 (1)	0.017 (1)	−0.006 (1)
C2	0.052 (2)	0.062 (2)	0.042 (2)	−0.014 (2)	0.024 (2)	−0.014 (2)
C3	0.087 (3)	0.073 (3)	0.057 (2)	−0.022 (2)	0.040 (2)	−0.018 (2)
C4	0.089 (3)	0.086 (3)	0.049 (2)	−0.025 (2)	0.038 (2)	−0.011 (2)
C5	0.065 (2)	0.096 (3)	0.039 (2)	−0.008 (2)	0.033 (2)	−0.002 (2)
C6	0.051 (2)	0.072 (2)	0.039 (2)	−0.005 (2)	0.025 (1)	−0.004 (2)
C7	0.081 (3)	0.056 (2)	0.056 (2)	−0.016 (2)	0.040 (2)	−0.026 (2)
C8	0.147 (4)	0.070 (3)	0.071 (3)	−0.019 (2)	0.074 (3)	−0.052 (3)
C9	0.131 (4)	0.140 (5)	0.089 (3)	−0.40 (3)	0.085 (3)	−0.084 (4)
C10	0.072 (3)	0.134 (4)	0.062 (3)	−0.023 (3)	0.049 (2)	−0.038 (3)
C11	0.053 (3)	0.196 (6)	0.056 (3)	0.002 (3)	0.019 (2)	0.018 (3)
C12	0.082 (3)	0.127 (4)	0.079 (3)	−0.002 (3)	0.043 (3)	0.035 (3)
C13	0.182 (5)	0.085 (3)	0.070 (3)	0.012 (3)	0.083 (3)	−0.011 (3)
C14	0.391 (9)	0.093 (4)	0.123 (5)	0.016 (4)	0.159 (5)	−0.030 (6)
C15	0.38 (1)	0.210 (7)	0.089 (4)	0.037 (6)	0.141 (7)	0.107 (7)
C16	0.125 (6)	0.36 (1)	0.087 (5)	0.006 (8)	0.054 (4)	0.070 (7)
C17	0.205 (8)	0.251 (8)	0.089 (4)	−0.036 (6)	0.079 (6)	−0.099 (6)

Table IV. Selected Bond Lengths and Bond Angles at Various Temperatures

	20 K[a]	128 K[a]	175 K[a]	298 K[a]	300 K[b]
		Bond Length, Å			
Fe(01)-N(01)	1.95 (1)	1.954 (5)	1.994 (6)	2.085 (7)	2.085 (3)
Fe(01)-N(02)	2.028 (9)	2.023 (5)	2.071 (6)	2.173 (8)	2.176 (3)
Fe(01)-O(01)	1.864 (8)	1.864 (4)	1.884 (5)	1.923 (5)	1.921 (2)
Fe(02)-N(21)	1.95 (1)	1.961 (5)	2.028 (6)		
Fe(02)-N(22)	2.037 (9)	2.032 (5)	2.095 (6)		
Fe(02)-O(21)	1.845 (8)	1.850 (4)	1.877 (5)		
		Bond angle, deg.[c]			
O(01)-Fe(01)-N(01)	91.4 (4)	90.5 (2)	89.6 (2)	87.2 (3)	87.2 (1)
O(01)-Fe(01)-N(02)	91.6 (3)	91.7 (2)	91.6 (2)	93.3 (3)	92.7 (1)
N(01)-Fe(01)-N(02)	85.1 (4)	85.0 (2)	84.3 (3)	82.1 (3)	83.0 (1)
O(21)-Fe(02)-N(21)	90.6 (4)	90.6 (2)	89.3 (2)		
O(21)-Fe(02)-N(22)	88.3 (3)	88.1 (2)	87.7 (2)		
N(21)-Fe(02)-N(22)	95.1 (4)	95.2 (2)	95.7 (3)		

[a] Performed at UCLA. [b] Performed at Illinois. [c] Bite angles for the (3-OEt-SalAPA) ligand.

benzene solvate molecule are located on twofold axes. The completely trans ligand atom configuration, predicted by Federer et al.[9] on the basis of intramolecular steric considerations and powder EPR data, is apparently stabilized by the propylene moiety that bridges the imine and amine nitrogen atoms. Analogous ferric N_4O_2 systems[26,27] with ethylene bridges are not centrosymmetric;

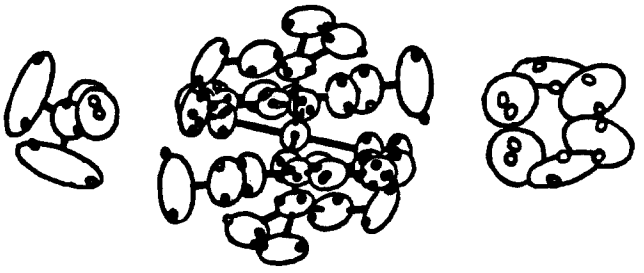

Figure 9. The relationship between the room-temperature ($C2/c$) and the low-temperature ($P2_1/c$) structures. Thermal ellipsoids from the room-temperature structure are superimposed with small circles that indicate the atomic positions at low temperature and the low-temperature positions translated by $(a + b)/2$. This figure suggests that the refined room-temperature thermal parameters mask a disorder of the two independent orientations observed at low temperature.

the two tridentate ligands coordinate meridionally with only the two imine nitrogen atoms trans.

The Fe–ligand bond lengths are in keeping with trends seen for other ferric N_4O_2 systems.[26-28] Specifically, the Fe–N(amine) bonds are longest, the Fe–O bonds shortest, and the Fe–N(imine) bonds intermediate. Moreover, these bond lengths are in good quantitative agreement with the room-temperature magnetic susceptibility (see Figure 1). Studies of analogous ferric N_4O_2 systems[28] have shown that the high- and low-spin electronic states exhibit average Fe–ligand bond lengths of 2.08 and 1.95 Å, respectively. The long Fe–N(amine) bond is the most spin-state dependent. The average Fe–ligand distance (2.061 Å) seen here corresponds to a high-spin fraction of 0.86, a value in excellent agreement with the high-spin fraction (0.85) calculated from the room-temperature magnetic susceptibility.

Powder X-ray diffraction data also confirm that the single crystal used in the X-ray diffraction experiments is identical with the microcrystalline material used in the magnetic and spectroscopic experiments. The experimentally determined d spacings are in excellent agreement with values calculated from the room-temperature unit cell parameters. Consequently, it is valid to relate the spectroscopic and magnetic data to the single-crystal structural results. The powder diffraction data and assignments are included as supplementary material.

The unit cell, illustrated in Figure 8, consists of well-isolated ionic and molecular units. There are no unusually short intermolecular contacts. It is evident in both Figures 7 and 8 that although the room-temperature structure refined to a low residual, abnormally large thermal parameters were obtained. Large ellipsoids are particularly evident for the benzene carbon atoms, two of the symmetry related perchlorate oxygen atoms, and the atoms of the ethoxy salicylaldehyde substituent. The structure determination at 128 K provides an explanation for this observation.

Low-Temperature Structural Results. A multiple-temperature structural investigation was undertaken in an effort to identify any structural features that might be associated with rapid spin-state interconversion. Three complete sets of low-temperature diffraction data were obtained, one at 128 K, one at 175 K, and one at ~20 K. Selected bond lengths and angles are listed in Table IV.

At 128 K the compound exhibits $P2_1/c$ space group symmetry, with two crystallographically-independent complex cations located on crystallographic inversion centers at 0, 0, 0, and $^1/_2$, $^1/_2$, 0. Superposition of the room-temperature structure, the low-temperature structure, and the low-temperature structure translated by $(a + b)/2$ in Figure 9 shows that for the anion, cation, and solvate molecule, the atomic displacements between the two

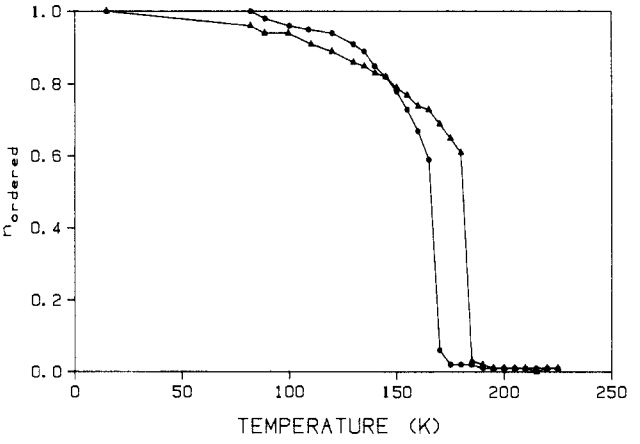

Figure 10. Temperature dependence of the average intensity of four symmetry-related reflections. n(ordered) = $I(T)/I(20\ K)$; $T_c \simeq 166$ K for heating (▲); $T_c \simeq 181$ K for cooling (●); $\Delta T = 15$ K.

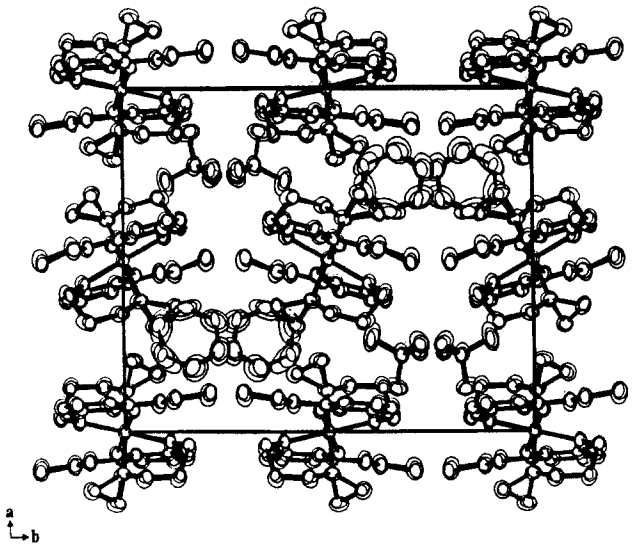

Figure 11. Superposition of the packing diagrams viewed down the c axis for the 20, 128, and 175 K structures.

low-temperature sites match in direction and magnitude the largest principal axes of the room-temperature thermal motion tensors. This suggests that the refined thermal parameters at room temperature mask a structural disorder. Additional measurements were undertaken to characterize further the nature of the $P2_1/c$ to $C2/c$ transformation.

The temperature evolution of the transition was mapped by following the intensity of the (−5, −2, 1) reflection and the three symmetry-related reflections as a function of temperature, both in the increasing and decreasing direction. These reflections are systematically absent in $C2/c$. Figure 10 shows a plot of the average intensity of these four reflections as a function of temperature. Between 80 and 150 K this intensity decreases in a fashion that suggests the onset of a second-order transition, but this decrease could also be a consequence of the spin-state transformation. In any event, the abrupt change above 180 K and the marked hysteresis ($\Delta T = 15$ K) indicate the presence of a significant first-order component to the transition.[29] ω scans of $h + k = 2n$ reflections in the hysteresis region show a splitting indicative of the presence of two phases. The structural determinations at 175 and ~20 K were undertaken to characterize more completely both the structural and spin-state transformations, and to study the relationship between them. In the case of the structural tansformation, it was of particular interest to follow the temperature dependence of the thermal parameters from very

(26) Sim, G.; Sinn, E.; Petty, R. H.; Merrill, C. L.; Wilson, L. J. *Inorg. Chem.* **1981**, *20*, 213.
(27) Timken, M. D.; Sinn, E.; Hendrickson, D. N. *Inorg. Chem.* **1985**, *24*, 3947.
(28) Ito, T.; Sugimato, M.; Ito, H.; Toriumi, K.; Nakayama, H.; Mori, W.; Sekizaki, M. *Chem. Lett.* **1983**, 121.
(29) Kittle, C.; Kroemer, H. "Thermal Physics"; W. H. Freeman Co.: San Francisco, 1980; p 304.

low temperature to just below the first-order transition. These observations could reveal any "soft mode" associated with a displacive transition. In addition, the Fe–ligand bond lengths obtained in these determinations can be used to monitor the spin-state transformation. While in other systems it has been possible to resolve the spin-state isomers as a function of temperature,[30] the complexity of this system and the nonrigid character of the ligands would make such a resolution very difficult in this case.

Figure 11 shows a superposition of a portion of the packing diagrams for the 20, 128, and 175 K structures. While there is an increase in the thermal motion with temperature, particularly for the perchlorate anion and benzene solvate molecule, there does not appear to be any abnormally large amplitude motion at 175 K that might be associated with a "soft mode".

Two observations related to the spin-state transformation are significant. First, the low-spin/high-spin ratios derived crystallographically from the average Fe–donor bond lengths are in good agreement with those derived from the magnetic susceptibility measurements (see Figure 1). Yet there is no indication of the abrupt structural transition in the magnetic susceptibility, Mössbauer, or EPR measurements; the thermodynamics of the spin-state equilibrium appear to be completely insensitive to the structural transformation. This probably indicates that the local environments of the iron(III) ions in the high-temperature phase are the same as those in the low-temperature phase, again consistent with an order–disorder rather than a displacive transition. If on this basis the high-temperature iron site is modeled as the superposition of the two low-temperature iron sites, $C2/c$ rather than Cc symmetry is required. This can be viewed as a very indirect resolution of the space group ambiguity for the high-temperature phase. In the absence of this restriction, since the transition is first order, there is no requirement that the inversion center in the low-temperature phase be preserved in the high-temperature phase. However, efforts to refine various models with Cc space group symmetry produced no significant improvement in the fit to the measured intensities.

A second crystallographic observation related to the spin transformation is that at 175 K the high-spin/low-spin ratios in the two crystallographically independent sites are 0.43 and 0.76 as determined by the iron–donor atom bond distances. This observation suggests a mechanism whereby dynamic interconversion between the two iron environments could influence the rate of spin-state interconversion.

Origins of Rapid Spin-State Interconversion. The primary motivation for this work was to identify factors that might be responsible for rapid spin-state interconversion rates in $[Fe(3\text{-}OEt\text{-}SalAPA)_2]ClO_4 \cdot C_6H_6$ and related spin-crossover solids. It is important to note that solution spin-crossover kinetics studies[31-33] have led to suggestions that intramolecular steric interactions play a significant role in determining spin-state interconversion rates. For the few solids for which both solution and solid-state spin-state interconversion rates have been determined,[31,34,35] the solid-state rates are consistently slower than the corresponding solution rates. Such observations have led Goldanskii[36] to suggest that lattice reorganizational energy results in large activation barriers to spin-state interconversion in the solid. In this view the "reorganization" is a local response of the lattice to a spin-state change. An alternative perspective in the analysis of the dynamics of the spin-state interconversion is to consider the response of the spin system to lattice dynamics. Dynamic structural interconversions of the type associated with the order–disorder transformation observed in this investigation could modulate the "ligand field" of the transition-metal ion and thereby enhance the rate of spin-state interconversion. (Notice that the "ligand field", as reflected in the crystallographically determined spin-state ratio, is different in the two iron sites.) Regardless of the perspective, a quantitative determination of the rates of both the structural and spin-state interconversion is required to substantiate the evidence of any coupling between the two processes.

The factors that influence the rate of spin-state interconversion may be related to the suggested origins for slow and rapid intramolecular electron-transfer rates in the mixed-valence trinuclear iron acetates.[37] Specifically, it has been suggested that a change in the electron-transfer rate in these materials is coupled to the onset of dynamic motion of a solvate molecule in the lattice; dynamic disorder in the lattice leads to rapid electron-transfer rates (relative to the Mössbauer spectroscopic time scale) and static order (or disorder) leads to slow rates. We are presently continuing our efforts to understand the role of lattice dynamics in determining the rates of intramolecular electron transfer and spin-state interconversion in molecular solids.

Acknowledgment. We are grateful for support from the National Institute of Health Grant HL13652 (D.N.H.) and from the National Science Foundation Grant CHE-8340836 (C.E.S.).

Supplementary Material Available: Tables of atomic positional and thermal parameters and observed and calculated structure factors for the X-ray structures; variable-temperature magnetic susceptibility data; variable-temperature Mössbauer data; figures of susceptibility and of Mössbauer data in the region of the order–disorder transition; X-ray powder diffraction data (84 pages). Ordering information is given on any current masthead page.

(30) Katz, B. A.; Strouse, C. E. *J. Am. Chem. Soc.* **1979**, *101*, 6214.
(31) Petty, R. H.; Dose, E. V.; Tweedle, M. F.; Wilson, L. J. *Inorg. Chem.* **1978**, *17*, 1064.
(32) Hoselton, M. A.; Drago, R. S.; Wilson, L. J.; Sutin, N. *J. Am. Chem. Soc.* **1976**, *98*, 6967.
(33) Dose, E. V.; Hoselton, M. A.; Tweedle, M. F.; Wilson, L. J.; Sutin, N. *J. Am. Chem. Soc.* **1978**, *100*, 1141.
(34) Tweedle, M. F.; Wilson, L. J. *J. Am. Chem. Soc.* **1976**, *98*, 4824.
(35) Dose, E. V.; Murphy, K. M.; Wilson, L. J. *Inorg. Chem.* **1976**, *15*, 2622.
(36) Goldanskii, V. I. *Pure Appl. Chem.* **1983**, *55*, 11.
(37) (a) Oh, S. M.; Hendrickson, D. N.; Hassett, K. L.; Davis, R. E. *J. Am. Chem. Soc.* **1984**, *106*, 7984. (b) Oh, S. M.; Kambara, T.; Hendrickson, D. N.; Sorai, M.; Kaji, K.; Woehler, S. E.; Witterbort, R. J. *J. Am. Chem. Soc.* **1985**, *107*, 5540. (c) Oh, S. M.; Hendrickson, D. N.; Hassett, K. L.; Davis, R. E. *J. Am. Chem. Soc.* **1985**, *107*, 8009. (d) Sorai, M.; Kaji, K.; Hendrickson, D. N.; Oh, S. M. *J. Am. Chem. Soc.*, in press.